A&A 638, A146 (2020)
https://doi.org/10.1051/0004-6361/202037552

Astronomy & Astrophysics

Optical validation and characterisation of *Planck* PSZ1 sources at the Canary Islands observatories

II. Second year of ITP13 observations

R. Barrena[1,2], A. Ferragamo[1,2], J. A. Rubiño-Martín[1,2], A. Streblyanska[1,2], A. Aguado-Barahona[1,2], D. Tramonte[1,2,3], R. T. Génova-Santos[1,2], A. Hempel[4,5], H. Lietzen[6], N. Aghanim[7], M. Arnaud[8,9], H. Böhringer[10], G. Chon[10], H. Dahle[11], M. Douspis[7], A. N. Lasenby[12,13], P. Mazzotta[14], J. B. Melin[8], E. Pointecouteau[15,16], G. W. Pratt[8,9], and M. Rossetti[17]

[1] Instituto de Astrofísica de Canarias, C/Vía Láctea s/n, 38205 La Laguna, Tenerife, Spain
e-mail: rbarrena@iac.es
[2] Universidad de La Laguna, Departamento de Astrofísica, 38206 La Laguna, Tenerife, Spain
[3] University of KwaZulu-Natal, Westville Campus, Private Bag X54001, Durban 4000, South Africa
[4] Universidad Andrés Bello, Departemento de Ciencias Físicas, 7591538 Santiago de Chile, Chile
[5] Max-Planck Institute for Astronomy, Königstuhl 17, 69117 Heidelberg, Germany
[6] Tartu Observatory, University of Tartu, 61602 Tõravere, Tartumaa, Estonia
[7] Institut d'Astrophysique Spatiale, Universitè Paris-Sud, CNRS, UMR8617, 91405 Orsay Cedex, France
[8] IRFU, CEA, Université Paris-Saclay, 91191 Gif-sur-Yvette, France
[9] Université Paris Diderot, AIM, Sorbonne Paris Cité, CEA, CNRS, 91191 Gif-sur-Yvette, France
[10] Max-Planck-Institut für extraterrestrische Physik, 85748 Garching, Germany
[11] Institute of Theoretical Astrophysics, University of Oslo, PO Box 1029, Blindern 0315, Oslo, Norway
[12] Astrophysics Group, Cavendish Laboratory, JJ Thomson Av., Cambridge CB3 0HE, UK
[13] Kavli Institute for Cosmology, Madingley Road, Cambridge CB3 0HA, UK
[14] Dipartimento di Fisica, Università degli Studi di Roma "Tor Vergata", via della Ricerca Scientifica, 1, 00133 Roma, Italy
[15] Université de Toulouse, UPS-OMP, Institut de Recherche en Astrophysique et Planétologie (IRAP), 31400 Toulouse, France
[16] CNRS, IRAP, 9 avenue Colonel Roche, BP 44346, 31028 Toulouse Cedex 4, France
[17] IASF-Milano, Istituto Nazionale di Astrofisica, via A. Corti 12, 20133 Milano, Italy

Received 22 January 2020 / Accepted 1 April 2020

ABSTRACT

We report new galaxy clusters previously unknown included in the first *Planck* Sunyaev–Zeldovich (SZ) sources catalogue, the PSZ1. The results presented here were achieved during the second year of a two-year observational programme, the ITP13, developed at the Roque de los Muchachos Observatory (La Palma, Spain). Using the 2.5 m *Isaac Newton* telescope, the 3.5 m Telescopio Nazionale *Galileo*, the 4.2 m *William Herschel* telescope and the 10.4 m Gran Telescopio Canarias we characterised 75 SZ sources with low SZ significance, SZ $S/N < 5.32$. We performed deep optical imaging and spectroscopy in order to associate actual galaxy clusters with the SZ *Planck* source. We adopted robust criteria, based on the 2D spatial distribution, richness, and velocity dispersions to confirm actual optical counterparts up to $z < 0.85$. The selected systems are confirmed only if they are well aligned with respect to the PSZ1 coordinate and show high richness and high velocity dispersion. In addition, we also inspected the Compton y-maps and SZ significance in order to identify unrealistic detections. Following this procedure, we identify 26 cluster counterparts associated with the SZ emission, which means that only about 35% of the clusters considered in this low S/N PSZ1 subsample are validated. Forty-nine SZ sources (~65% of this PSZ1 subset) remain unconfirmed. At the end of the ITP13 observational programme, we have studied 256 SZ sources with Dec $\geq -15°$ (212 of them completely unknown), finding optical counterparts for 152 SZ sources. The ITP13 validation programme has allowed us to update the PSZ1 purity, which is now more refined, increasing from 72% to 83% in the low SZ S/N regime. Our results are consistent with the predicted purity curve for the full PSZ1 catalogue and with the expected fraction of false detections caused by the non-Gaussian noise of foreground signals. We find a strong correlation between the number of unconfirmed sources and the thermal emission of diffuse galactic dust at 857 GHz, thus increasing the fraction of false *Planck* SZ detections at low galactic latitudes.

Key words. large-scale structure of Universe – galaxies: clusters: general – catalogs

1. Introduction

Galaxy clusters are extraordinarily useful when studying the structure and evolution of the Universe. The Λ cold dark matter (ΛCDM) cosmological model makes accurate predictions on the number, abundance, and distribution of galaxy clusters throughout the Universe, making it evident that galaxy clusters play an important role in constraining cosmological models (e.g. Evrard 1989; Henry & Arnaud 1991; White et al. 1993; Eke et al. 1996; Donahue et al. 1998; Borgani & Guzzo 2001). Moreover, cluster abundance studies as a function of mass and redshift, $N(M,z)$, are powerful cosmological probes (Carlstrom et al. 2002; Allen et al. 2011), allowing us to set constraints on parameters such as the dark matter and dark energy densities (ρ_{DM}, ρ_{Λ}) or the

equation of the state of the dark energy (w) (Vikhlinin et al. 2009; Mantz et al. 2010).

Throughout the past decades, large-area sky surveys have identified tens of thousands of galaxy clusters by using different techniques such as selecting overdensities of galaxies in optical (e.g. Abell 1958; Abell et al. 1989; Postman et al. 1996; Wen et al. 2009, 2012) and infrared (e.g. MaDCoWS Gonzalez & Gettings 2019) surveys, detecting diffuse X-ray sources (e.g. Ebeling et al. 1998; Böhringer et al. 2000), tracing the mass gravitational effect produced by the weak-lensing footprint (e.g. Wittman et al. 2006), and, very recently, disentangling the Sunyaev–Zeldovich (SZ) effect on the Cosmic Microwave Background (CMB) maps.

The SZ effect (Sunyaev & Zeldovich 1972) is produced through the inverse Compton scattering when CMB photons interact with the high-energy electrons of hot intracluster gas, which yields a spectral distortion in the CMB. This effect has been used to detect galaxy clusters in ground-based millimetre wave surveys, such as the Atacama Cosmology Telescope (ACT; Swetz et al. 2011) and the South Pole Telescope (SPT; Carlstrom et al. 2011). More recently, the *Planck*[1] satellite (Planck Collaboration I 2014) provided full sky coverage and the opportunity to detect galaxy clusters through the SZ effect (Planck Collaboration VIII 2011; Planck Collaboration XXIX 2014; Planck Collaboration XXVII 2016). The results of the *Planck* SZ survey have been published in two catalogues, the first public SZ catalogue (PSZ1; Planck Collaboration XXIX 2014; Planck Collaboration XXXII 2015) and the second public SZ catalogue (PSZ2; Planck Collaboration XXVII 2016).

Using the SZ effect to detect galaxy clusters has the main advantage that the surface brightness of SZ signal does not decay with the redshift. This allows us to detect massive clusters at any redshift. The combination of the PSZ1 and PSZ2 catalogues provides 1943 unique SZ detections with 1330 confirmed clusters and 613 unconfirmed sources. However, in order to make these cluster samples useful for cosmology, it is essential to characterise and have an accurate knowledge of the *Planck* SZ sensivity and detection purity.

In 2010 the *Planck* collaboration started to confirm SZ cluster candidates cross-correlating with previous existing cluster catalogues. The search for possible SZ cluster candidates began with the MCXC catalogue (Piffaretti et al. 2011) and the AllWISE mid-infrared source catalogue (Cutri et al. 2012). Today, many efforts have been made to confirm SZ sources at optical wavelengths. Examples of these programmes are those performed using the DSS[2] images, the SDSS-DR8 survey (Aihara et al. 2011) and the WISE all-sky survey (Wright et al. 2010). In addition, the PSZ1 catalogue was cross-correlated to X-ray data, mainly with the ROSAT All Sky Survey (Voges et al. 1999, 2000), as well as other SZ catalogues derived from SPT (Bleem et al. 2015) and ACT maps (Marriage et al. 2011). Later, several optical follow-up programmes were carried out using large telescopes by obtaining new deep images and spectra. This is the case of the programmes performed with the RTT150 telescope (Planck Collaboration Int. XXVI 2014), and the ITP13 (Planck Collaboration Int. XXXVI 2016; Barrena et al. 2018, hereafter B+18).

Thus, SZ surveys provide a very valuable tool for constructing cluster samples almost complete in mass. However, these samples can be used to determine cosmological parameters and restrict cosmological models only if their selection functions are well determined. As SZ surveys only provide flux determinations, systematic follow-up programmes of SZ sources are essential in order to carry out the scientific exploitation of the resulting catalogues. This is the main goal of this work and, in general, the main aim of the ITP13 validation programme, thus providing a full characterisation of unknown SZ sources of the PSZ1 catalogue.

This paper is the third of the series and the last work in the framework of the International Time Project (ITP13), a follow-up programme carried out in the Canary Islands Observatories, dedicated to confirming and characterising the PSZ1 sources. The ITP13 began with the Planck Collaboration Int. XXXVI (2016) and followed with B+18. This set of papers includes a detailed study of a complete sample of 212 unknown PSZ1 sources with Dec $\geq -15^\circ$ that constitutes the ITP13 sample. Here, we present deep photometric and spectroscopic data of a sample of 75 SZ sources classifying them as actual cluster counterparts or unconfirmed detections with no optical counterpart. The main aim of the ITP programme is to improve the knowledge of the initial *Planck* SZ completeness, purity, and selection function in order to obtain a clean PSZ1 sample useful for cosmological studies.

In a similar way, very recently, several optical follow-ups have been focused on PSZ2 sources. Examples of these observational programmes include one performed by van der Burg et al. (2016) (hereafter vdB+16) using the MegaCam at CFHT, one realised by Streblyanska et al. (2018) using the SDSS-DR12 database, one carried out using the 4.2 m *William Herschel* Telescope by Zohren et al. (2019), and one by Boada et al. (2019) using the 4 m Mayall telescope from Kitt Peak National Observatory. Complementary to this ITP13, we also carried out a second optical follow-up (the LP15 long-term observational programme) in order to validate the unknown SZ sources of the PSZ2 catalogue using the facilities at the Roque de los Muchachos Observatory (ORM). We have characterised 190 PSZ2 sources with Dec $> -15^\circ$ studying the purity of this sample. The results of these works have been published in Streblyanska et al. (2019) and Aguado-Barahona et al. (2019).

This paper is organised as follows. Section 2 describes the observational strategy, and Sect. 3 includes details on the cluster detection technique and validation criteria. Section 4 provides the cluster counterpart catalogue of SZ sources studied in this work, as well as a discussion on the nature of some particular cases. Section 5 summarises the whole ITP13 programme providing results on the purity and completeness of the northern PSZ1 sample, and we will expose a possible explanation for a such large number of unconfirmed SZ sources. Finally, Sect. 6 presents the conclusions.

Throughout this paper, we assume a ΛCDM cosmology, taking $H_0 = 100\,h\,\mathrm{km\,s^{-1}\,Mpc^{-1}}$, with $h = 0.70$, $\Omega_\mathrm{m} = 0.3$, and $\Omega_\Lambda = 0.7$.

2. PSZ1 and observational strategy

2.1. PSZ1 catalogue and ITP13 subsample

The PSZ1 catalogue (Planck Collaboration XXIX 2014; Planck Collaboration XXXII 2015) includes 1227 sources selected from SZ effect detections using all-sky maps obtained during the first 15.5 months of *Planck* observations. Very briefly, SZ sources

[1] *Planck* (http://www.esa.int/Planck) is a project of the European Space Agency (ESA) with instruments provided by two scientific consortia funded by ESA member states and led by principal investigators from France and Italy, telescope reflectors provided through a collaboration between ESA and a scientific consortium led and funded by Denmark, and additional contributions from NASA (USA).

[2] DSS: http://stdatu.stsci.edu/dss

were selected using two Multi-Matched Frequency methods (the MMF1 and MMF3) and the PowellSnakes (PwS) technique (see Melin et al. 2012) with a signal-to-noise ratio (S/N) of 4.5 or higher. A total of 74% of the PSZ1 catalogue have been validated, determining redshifts for 913 systems, of which 736 are spectroscopic; 753 cluster candidates correspond to PSZ1 with Dec > −15°, which define the PSZ1 reference sample visible from Canary Island observatories (hereafter the PSZ1-North sample); 541 of the 753 PSZ1 sources have been validated through several follow-ups, while the remaining 212 SZ candidates form the ITP13 sample. Planck Collaboration Int. XXXVI (2016) and B+18 have studied 185 PSZ1 targets, some of them already known but without spectroscopic information. In this work we complete the study of unknown PSZ1 sources characterising the remainning 75 fields. The majority of SZ sources characterised during the ITP13 programme show a low S/N in the SZ detection, as expected for unknown sources. Only the 12% present $S/N > 6$.

2.2. Optical follow-up observations

The International Time Project ITP13 was a two-year observational campaign carried out at the ORM on the island of La Palma (Spain) from August 2013 to July 2015. Barrena et al. (2018) reported the optical characterisation of 115 SZ sources (with confimed and unconfirmed counterparts) observed during the first year of the ITP13 programme. In the present work, we report the optical validation carried out in the second and last year, from August 2014 to July 2015.

Table 1 lists the telescopes and instruments used to obtain the photometry and spectroscopic observations. We used four telescopes: the 2.5 m *Isaac Newton* Telescope (INT) and the 4.2 m *William Herschel* Telescope (WHT) operated by the Isaac Newton Group of Telescopes (ING), the 3.5 m Italian Telescopio Nazionale *Galileo* (TNG) operated by the Fundación Galileo Galilei of the INAF (Istituto Nazionale di Astrofisica), and the 10.4 m Gran Telescopio Canarias (GTC) operated by the Instituto de Astrofísica de Canarias (IAC). The 2.5 m INT and 4.2 m WHT were used to obtain deep images around SZ *Planck* pointings, while we performed the spectroscopic validation with the 3.5 m TNG and 10.4 m GTC telescopes using their respective multi-object spectrographs.

In order to configure the imaging and spectroscopic sample, we searched for possible SZ counterparts in the Sloan Digital Sky Survey (SDSS)[3] and the Digitized Sky Survey (DSS)[4]. The positive identifications of this previous screening were directly selected for spectroscopic observations. On the other hand, SZ sources with no clear cluster counterparts in the public DSS and SDSS data were included in the sample to obtain images with the INT and WHT telescopes, which allowed a deeper inspection.

Following the same scheme presented in B+18, and after a previous screening of DSS and SDSS data, the observational strategy followed two steps. First, unknown PSZ1 sources were observed by obtaining g', r', and i' deep images; then, if SZ counterparts were identified as galaxy overdensities, they were confirmed through multi-object spectroscopy (MOS) observations. So, clusters were definitely confirmed as actual SZ counterparts and directly linked to the PSZ1 source according to the distance to the *Planck* pointing, richness, and velocity dispersion (see Sect. 3).

[3] http://skyserver.sdss.org
[4] http://archive.stsci.edu/dss

2.2.1. Imaging observations, data reduction, and photometry

The High Frequency Instrument (HFI) *Planck* data provides maps that extend from 100 to 857 GHz, with different beam sizes that vary from 9.6′ at the lowest frequencies to 4.5′ at the highest. The positional error for detecting SZ source using *Planck* maps is thus about 2′ for targets in the PSZ1 sample (Planck Collaboration XXIX 2014). This result has been confirmed by comparing *Planck* SZ and REFLEX II sources. Böhringer et al. (2013) found an offset smaller than 2′ between X-ray and SZ centres. Furthermore, Planck Collaboration Int. XXXVI (2016) and B+18 found typical offsets of about 2.4′ and 2.8′, respectively, by comparing the positions of optical and SZ centres of PSZ1 sources. On the other hand, for PSZ2 counterparts, Streblyanska et al. (2018), Streblyanska et al. (2019), and Aguado-Barahona et al. (2019) also found offsets between 2.6′ and 4.4′. Thus, imaging cameras with fields of view (FOV) larger than ∼8′ × 8′ are suitable to observe the sky areas containing *Planck* SZ counterparts. Therefore, we carried out imaging observations using the Wide field Camera (WFC) and the Auxiliary Port Camera (ACAM), respectively, which provide a FOV of 34′ × 34′ and 4′ radius.

We typically acquire 1500 s and 900 s exposures in each band using the WFC and ACAM cameras. A small dithering pattern consisting of three frames with ∼10″ offset was performed in order to remove bad pixels, cosmic rays, and vignetting zones from the CCD frames. We obtain deep imaging in g', r', and i' broad-band filters obtaining ∼5σ and 3σ detection levels at magnitudes $r' = 21.8$ and 23.2 mag, respectively, using the WFC, and $r' = 22.0$ and 23.8 mag in the ACAM frames.

The optical WFC and ACAM images were reduced using standard IRAF tasks[5]. Raw WFC and ACAM data were corrected from bias and flat-field effects. Additionally, the final images were calibrated astrometrically by using `images.imcoords` IRAF tasks obtaining a precison of ∼0.1″ across the vast majority of the image. Deviations of ∼1″ are only present at the edge of the FOV. The photometric calibration was based on SDSS-DR12 standard fields.

We use `SExtractor` (Bertin & Arnouts 1996) in single-image mode in order to perform the source detection and photometry, following the same scheme as in B+18. Objects were detected if they extended more than 10 pixels showing $S/N > 3\sigma$ in each of the g', r', and i' frames. The `MAGAUTO` procedure was applied to obtain photometry in elliptical apertures. Then, the individual g', r', and i' photometric catalogues were merged into a master catalogue to include the three-band photomety. This merging was done by searching for matchings within 1″ apertures.

The WFC presents large PSF distortions over the full FOV. This made difficult to distinguish between star and galactic shapes, in particular for sources fainter than $r' = 18$ mag. So, we only carried out star-cleaning procedures statistically assuming that cluster regions and the background around them show the same distribution of point sources. This step was crucial in order to obtain a realistic richness and clear red sequences (hereafter RSs) in the colour–magnitude diagrams (CMDs).

All the images obtained in the ITP13 programme are included in the Virtual Observatory collection and are publicly available. In the near future, the photometric and spectroscopic catalogues will be also accessible through this web platform.

[5] IRAF (http://iraf.noao.edu/) is distributed by the National Optical Astronomy Observatories, which are operated by the Association of Universities for Research in Astronomy, Inc., under cooperative agreement with the National Science Foundation.

Table 1. Telescopes and instruments used in the second year of observations of the ITP13 programme.

Telescope	Instrument	FoV	Pixel scale [″]	Resolution	$N_{\rm ima}$	$N_{\rm spec}$
2.5 m INT	WFC	$34' \times 34'$	0.33	–	38	
3.6 m TNG	DOLORES	$8\farcm6 \times 8\farcm6$	0.252	$R = 600$		10
4.2 m WHT	ACAM	$4'$ radius	0.253	$R = 400$	33	2
10.4 m GTC	OSIRIS	$7\farcm8 \times 7\farcm8$	0.254	$R = 500$	1	15

2.2.2. Spectroscopic observations and data reduction

The majority of the spectra obtained in this observational campaign were acquired using the MOS devices of DOLORES and OSIRIS spectrographs at the 3.5 m TNG and the 10.4 m GTC, respectively. Only a few spectra were obtained using long-slit configuration of OSIRIS, which allowed us to include a few galaxies in each acquisition. The long-slit exposures were acquired using the same instrument set-up as for the MOS mode. The technical details of these instruments are specified in B+18. The two instruments, with a FoV of $\sim 7' \times 6'$, allowed us to sample $\sim$1 Mpc radius, which represent typically about 1 $R_{\rm vir}$ of a cluster at $z \sim 0.3$. For closer clusters, only the inner regions were sampled, while for distant clusters we even obtained spectra in their outer regions.

As in the first year of observations (B+18), we acquired three exposures of 1800 s per mask and cluster using DOLORES/TNG and 3×1000 s acquisitions through DOLORES/GTC. These integration times, and a typical seeing of $\sim 1.1''$, allowed us to obtain $S/N \sim 5$ in the spectra of galaxies with magnitudes $r' = 20.5$ and 21.5 in the TNG and the GTC, respectively.

The mask configuration was performed on previous images for each field, placing about 40 slitlets in DOLORES masks and about 50 slitlets in OSIRIS masks. Galaxy targets (likely cluster members) were selected from the colour magnitudes obtained with ACAM and WFC photometry. In addition, we used RGB colour composite images built from g'-, r'-, and i'-band frames as references. Basically, we selected likely cluster members, that means galaxies with coherent colours, consistently with the redshift of the cluster and contained within its RS.

The raw spectra were reduced using standard IRAF tasks. DOLORES and OSIRIS spectrographs present a very good and flat spectral response. For this reason, and in order to avoid degrading the S/N, bias and flat-field correction were not applied. Only sky subtraction, extraction of spectra, wavelength calibration (using He-Ne, Hg, and Ar arcs), and cosmic ray rejection procedures were performed. Finally, we checked the OI telluric line (5577.3 Å) looking for possible deviations. We found small offsets ($\sim$1 Å, i.e. $\sim$50 km s^{-1} offset in velocity) in some masks due to flexures of the optical system while acquiring data. Spectra were corrected for this effect.

The final scientific spectra showed $S/N \sim 5$ (per pixel around 5000 Å) for galaxies $r' \sim 20.5$ and 21.7 mag, observed with the DOLORES/TNG and OSIRIS/GTC, respectively. In order to optimise the telescope time, we observed nearby clusters ($z_{\rm phot} \lesssim 0.35$) in the TNG telescope, while distant clusters (with $z_{\rm phot} \gtrsim 0.35$) were included in the target list for the GTC. Figure 1 shows two spectra of galaxy cluster members obtained with OSIRIS/GTC and DOLORES/TNG.

The redshift determination of galaxies were obtained using the correlation technique of Tonry & Davis (1979) provided by the `RVSAO/IRAF`[6] package and the `XCSAO` and `EMSAO` tasks. This procedure correlates the scientific spectra with several spectrum templates assigning an R parameter associated with the quality of the process. We use six spectrum templates of different galaxy morphologies, from ellipticals to irregulars, where `XCSAO` and `EMSAO` were able to identify the main absorptions (H and K doublet, G-band and MgI triplet) and emission features (mainly OII, OIII doublet, H_β and H_α lines). We select the redshift estimation corresponding to the highest R-value, rejecting estimates with $R < 2.8$, which show errors that are too high (>150 km s^{-1}), so they correspond to unreliable determinations. Errors in the redshift estimates were $\Delta v \sim 80$ km s^{-1}. However, by comparing a set of about 30 spectra with redshifts also available in the SDSS-DR12 archive, we estimate the systematic errors $\Delta v = 110$ km s^{-1}, which is appropriate to sample the velocity dispersion of massive clusters with $\sigma_v > 500$ km s^{-1}.

As in B+18, we perfom multi-object spectroscopy, which is the ideal technique for sampling the galaxy members in the dense environments of cluster cores. The DOLORES/TNG and OSIRIS/GTC spectrographs allowed us to obtain up to 45 and 60 redshifts per mask, respectively, and so we were able to retrieve 10–25 galaxy members per cluster. The success rate[7] varies from 80% to 5%, with a mean of $\sim$40%, depending on the sampled region (the core or external zones) and the redshift of the cluster. Only a very small fraction ($\sim$2%) of the targets observed turned out to be stars, mainly red objects fainter than $r' = 21$.

The galaxy member selection was carried out in two steps: first, we consider galaxy cluster members only if they showed radial velocities in the range ± 3000 km s^{-1} with respect to the main value obtained for all galaxies in the cluster; second, we iterate the process by selecting galaxies only if they show radial velocities within $\pm 2.7\sigma_v$ with respect to the mean cluster redshift. This sigma-clipping selection minimises, as much as possible, the contamination by interlopers (Mamon et al. 2010).

3. Cluster identification and confirmation criteria

The main idea behind the cluster identification is to detect overdensities in galaxy distributions as the signature of mass concentration. However, given that the galaxy population in massive clusters is dominated by early-type morphologies, we look for galaxy overdensities showing coherent colours, the RS in the CMD (Gladders & Yee 2000). This method allows us not only to detect clusters, but also determine their photometric redshifts. Following the same prescription detailed in B+18, we selected likely galaxy members in the $(g' - r', r')$ and $(r' - i', r')$ CMDs. We identify the brightest cluster galaxy (BCG) and we fit the RS considering the five brightest likely cluster members with respect to the colour of the BCG in $g' - r'$ or $r' - i'$. Thus, the photometric redshift of clusters is derived using the mean colour of likely members (assumed as galaxies with the $RS \pm 0.15$; see Fig. 2)

[6] RVSAO was developed at the Smithsonian Astrophysical Observatory Telescope Data Center.

[7] Percentage of cluster members obtained with respect to the whole target observed in a region.

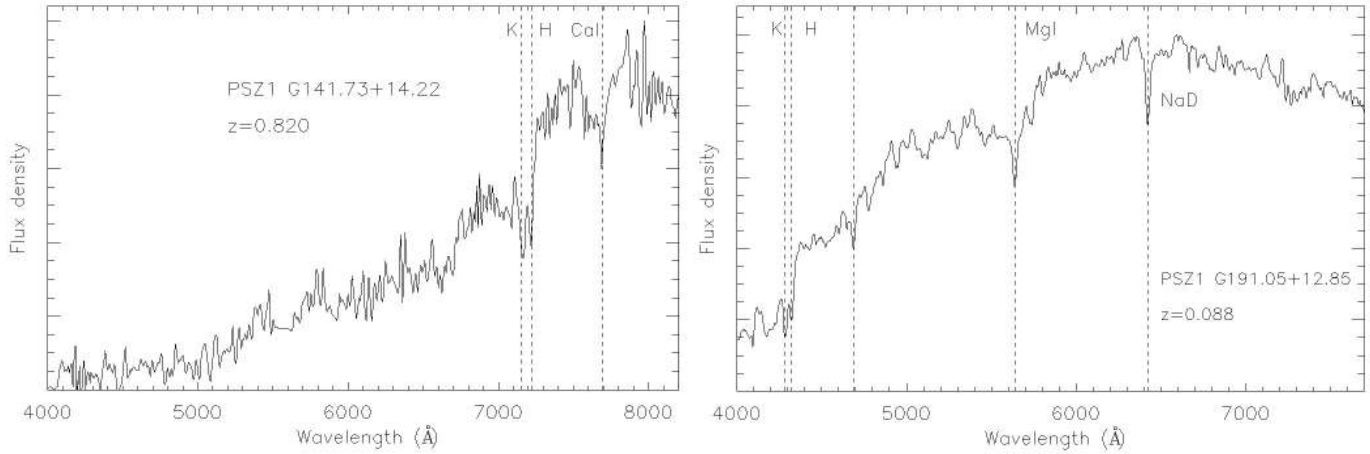

Fig. 1. Example of the spectra obtained with GTC/OSIRIS (*left panel*) and TNG/DOLORES (*right panel*) for the two brightest cluster galaxies, G141.73+14.22 and G191.05+12.85, at $z = 0.8208$ and 0.0895, with magnitudes $r' = 21.9$ and 14.8, respectively. Vertical dashed lines mark the absorption features identified at the redshift of the clusters.

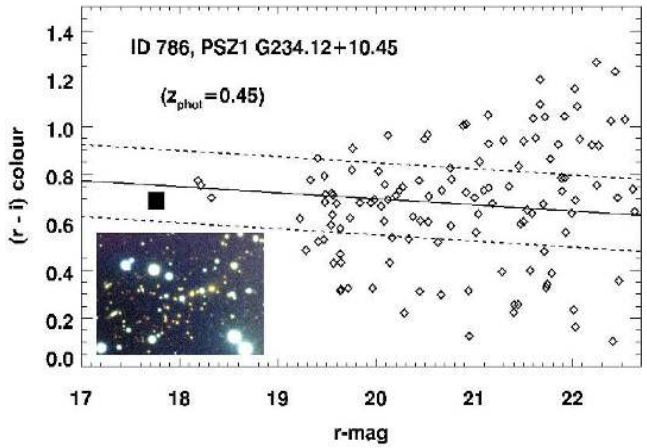

Fig. 2. $(r' - i', r')$ CMD of the source PSZ1 G234.12+10.45. Only extended sources within a region of 3×2.5 (~1.3×1.1 Mpc) around the BCG (large filled square) are considered. The RS (solid line) fit yields a $z_{\rm phot} = 0.45$. Dashed lines limit the $RS \pm 0.15$ mag of likely cluster members. A colour composite image (built using the g', r', and i' frames with $3' \times 2.5'$ FOV) is shown superimposed on the diagram.

and the Eqs. (1) and (2) from Planck Collaboration Int. XXXVI (2016). Therefore, this process allows us to select cluster member candidates to configure a sample of targets for further MOS observations.

We also use RGB colour composite images, constructed by the combination of g'-, r'-, and i'-frames to confirm our findings. The galaxy clumps, dominated by a population of early-type galaxies, is clearly visible in the field. In this way, the visual inspection of RGB images proved to be very efficient in cluster identification, in particular for clusters at $z > 0.7$ where only a few bright galaxies can be detected and the corresponding RS was not evident. In addition, fossil systems (e.g. Jones & Ponman 2003; Voevodkin & Borozdin 2010) are special cases, with a core dominant (cD) galaxy surrounded by a population of small galaxies, showing a two-magnitude gap with respect to the cD. This means that their RS is not as populated as for normal clusters at the bright end, making these systems difficult to characterise. Therefore, in the case of fossil clusters, the visual inspection of RGB images turns out to be very useful.

Confirmation criteria. The cluster identification is performed following robust confirmation criteria. We select clusters associated with SZ emissions assuming two premises. First, clusters have to be well aligned with the SZ peak. Second, clusters showing a SZ signal in *Planck* maps are expected to be massive systems. The first condition is related to the distance between the *Planck* pointing and the optical centre of the clusters. We assume that valid clusters should be placed at <5′, which means 2.5 times the typical positional error in the position of *Planck* SZ detections. This is in agreement with the findings obtained by Böhringer et al. (2013), Planck Collaboration Int. XXXVI (2016), and B+18. The second condition is related to the mass of the clusters. Poor systems, groups of galaxies, do not have enough mass content to able to generate a significant SZ signal in *Planck* maps.

So, from Planck Collaboration XXIV (2016) (see Fig. 1 therein) we assume that *Planck* SZ clusters should present masses $M_{500} \gtrsim 2\ 10^{14}\ M_\odot\ h_{70}^{-1}$ if they are at $z > 0.2$ or $M_{500} \gtrsim 10^{14}\ M_\odot\ h_{70}^{-1}$ if they are nearby structures ($z < 0.2$). These mass values can be interpreted in terms of velocity dispersion, which can be estimated because we have spectroscopic information for a suficient number of cluster members. Therefore, given the relation between M_{500} and σ_v by Munari et al. (2011), we assume valid SZ counterparts that clusters at $z < 0.2$ showing $\sigma_v > 500\,{\rm km\,s^{-1}}$ ($M_{500} > 10^{14}\ M_\odot\ h_{70}^{-1}$) and $\sigma_v > 650\,{\rm km\,s^{-1}}$ ($M_{500} > 2 \times 10^{14}\ M_\odot\ h_{70}^{-1}$) for clusters at $z > 0.2$.

However, in cases where we have no spectroscopic information, we confirm cluster candidates using the "richness significance". In other words, in the absence of σ_v information, galaxy overdensities are considered actual SZ counterparts only if they are rich clumps. A detailed description of the method used here to compute the richness significance is shown in Streblyanska et al. (2019). Briefly, for each cluster we count first the likely cluster members (assumed as galaxies within the $RS \pm 0.15$, in colour) showing r'-magnitudes in the range $[m_\star - 1, m_\star + 1.5]$ and lying within 1 Mpc of the cluster centre, R_0. Then, in order to decontaminate this estimate from the field galaxy contribution, we also estimate the richness of the outer regions, R_f. Finally, we substract it from the original estimate leading to the value $R_{\rm cor} = R_0 - R_f$. However, we base our confirmation criterion on the significance above the background level σ_R, which is computed as $R_{\rm cor}/\sqrt{R_f}$. An example of the latter is

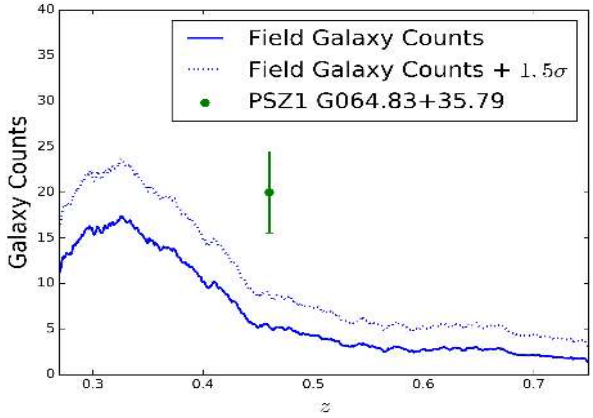

Fig. 3. Galaxy counts in the field of PSZ1 G064.83+35.79 as a function of the redshift (solid line) and its corresponding $+1.5\sigma$ error (dotted line). For this particular case, the richness, represented by the green point in the plot, is computed using the $(r' - i', r')$ CMD, thus obtaining a $\sigma_R = 6.5$ from likely members within 1 Mpc of the cluster center.

Table 2. Confirmation criteria adopted to validate or reject clusters as counterparts of SZ detections.

Flag	Spectroscopy	σ_v limit (km s^{-1})	σ_R	Dist.
1	YES	>500; $0 < z < 0.2$	>1.5	<5′
		>650; $z > 0.2$	>1.5	<5′
2	NO	NA	>1.5	<5′
3	YES	<500; $0 < z < 0.2$	>1.5	<5′
		<650; $z > 0.2$	>1.5	<5′
	NO	–	<1.5	>5′
ND	Non-detection ≡ No galaxy overdensity			

shown in Fig. 3. Table 2 summarises the conditions imposed in order to confirm the clusters as actual SZ counterparts.

For several particular cases, we observe SZ cluster candidates using the ACAM/WHT imaging camera. Given that this camera presents a small format FOV, only the inner region of the clusters can be sampled, while the galaxy background around that could not be estimated. Therefore, in order to correct the galaxy counts in the cluster region (R_0), from the field contribution (R_f), we make a master background of the average of the fields observed, but excluding a region of 0.5 Mpc radius from those fields where a cluster has been detected. These galaxy counts, extracted from the master background, were used to compute individual R_f values according to the different redshifts of the clusters, and so to obtain individual σ_R estimates for the clusters observed with the ACAM/WHT camera.

In the present work, the optical cluster centres are assumed to be the BCG position. However, in the cases showing no evident BCG, the optical centre is supposed to be the centroid (the mean position coordinates) of likely members. So, we adopt a confirmation criteria based on the distance (<5′), computed as the projected angle between optical centre and SZ peak emission.

Following the criteria given above, based on velocity dispersion, richness significance (as mass tracers), and distance to the SZ peak emission, the cluster counterparts are classified in three different categories, labelled `Flag`=1, 2, and 3, according to their validation level. Therefore, clusters classified as `Flag`= 1 correspond to massive, rich, and well-aligned systems confirmed spectroscopically, while clusters classified as `Flag`= 2 are also considered SZ counterparts, but only photometrically. For such cases, no spectroscopic information has been obtained; however, the detections show richness significance ($\sigma_R > 1.5$). Clusters labelled `Flag`= 2 may be observed spectroscopically in future works, and so consequently modify their `Flag` classification. Clusters classified as `Flag`=3 correspond to galaxy systems not closely associated with the SZ emission. They could be poor systems, confirmed spectroscopically as group-like systems showing low velocity dispersion, and/or systems very distant (>5′) from the *Planck* pointing. Thus, we assume these clusters as not valid SZ counterparts. Finally, the 'ND' label corresponds to fields where no galaxy overdensity has been detected, that is fields where σ_R shows no significant peak, $\sigma_R < 1.5$.

4. Results

Table A.1 lists the results for the 75 PSZ1 sources analysed in this work and is organised as follows. The first four columns show the identification number in the PSZ1 and PSZ2 lists, the *Planck* official name, and the significance of the SZ detection reported in the PSZ1 catalogue, respectively. Columns 5 and 6 provide the equatorial coordinates (J2000) of the optical centre (assumed the BCG position in the most of the cases) of cluster counterparts, while Col. 7 reports the distance between this centre and the SZ centre. The double column, Col. 8, lists the mean spectroscopic redshift of the clusters and that corresponding to the BCG (if available or present). Column 9 records the number of spectroscopic redshifts obtained for cluster members. Column 10 reports the photometric redshift, and the multiple column 11 shows the richness and richness significance obtained for each clump. Column 12 provides a `Flag` assignment according to the validation criteria. The last column includes notes relative to several cluster counterparts.

In agreement with Sect. 2.2.2, the $z_{\rm spec,BCG}$ presents a mean error of $\Delta z = 0.0004$. However, effects such as the low number of cluster members considered, the presence of substructures, and possible interlopers may produce a mean error in the $<z_{\rm spec}>$ determination of $\Delta z \sim 0.001$.

Following the confirmation criteria detailed in the previous section, we find that 26 out of 75 SZ sources analysed present reliable cluster counterparts, 16 of them are definitely confirmed spectroscopically (classified with `Flag`=1), and 10 (with `Flag`= 2) are very rich and reliable and are awaiting spectroscopic confirmation. On the other hand, almost two-thirds of the sample (49 out of 75 sources) show no cluster counterparts: 12 sources (with `Flag`=3) are poorly associated with their corresponding SZ signal and 37 are fields where no galaxy overdensity has been found (labelled "ND").

We report spectroscopic information for 29 clusters, 21 of which were observed in MOS mode, using DOLORES and OSIRIS spectrographs. The remaining eight clusters were spectroscopically studied in long-slit configuration of ACAM, or were prospected using public data from SDSS-DR12 archive. The physical parameters of the clusters used here for the confirmation criteria, such as the velocity dispersions and dynamical masses, will be reported and discussed in a future paper Ferragamo et al. (in prep.).

In the following subsections we analyse the precision of SZ centres, agreement between photometric and spectroscopic redshift, and we discuss on the nature of some clusters showing particularities, such as fossil clusters or the presence of strong gravitational lensing effects (gravitational arcs and arclets; see e.g. Fort et al. 1986; Soucail et al. 1987).

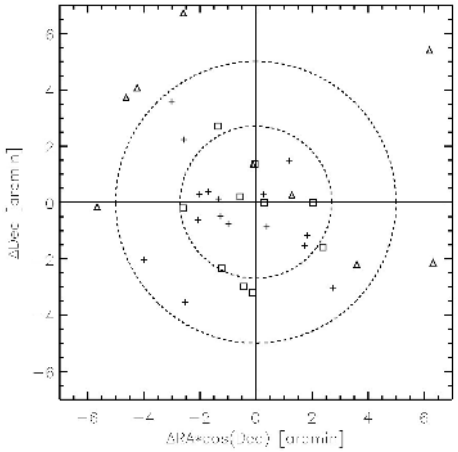

Fig. 4. Spatial distribution of optical centres with respect to their corresponding PSZ1 coordinates. Crosses, squares, and triangles correspond to clusters flagged as 1, 2, and 3, respectively. The inner dashed circle marks the 2.8′ radius region where 68% of the confirmed clusters are enclosed. The external dashed circle corresponds to the beam size (5′) of SZ *Planck* detections.

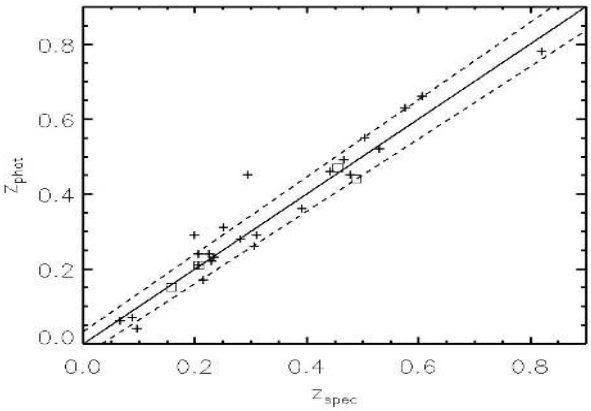

Fig. 5. Comparison between photometric and spectroscopic redshifts for all the clusters characterised in this work and detailed in Table A.1. The solid line shows the 1:1 relation and dashed lines represent the photometric redshift error $\delta z/(1+z) = 0.03$. Crosses represent photometric redshifts obtained using our INT and WHT photometry. Squares are redshifts retrieved from SDSS-DR12 archive.

4.1. Precision of SZ coordinates and redshifts

Figure 4 shows the spatial distribution of the optical centres of clusters relative to the PSZ1 coordinates. Ten clusters out of 26 showing actual counterparts present centres closer than 2′ to the PSZ1 coordinate. Moreover, 68% of the clusters are enclosed within 2.8′, which is in agreement with the finding of 2′ obtained in the REFLEX II X-ray follow-up of *Planck* SZ sources.

By comparing the photometric and spectroscopic redshifts of the clusters listed in Table A.1, we analyse the reliability of the photometric redshift estimates (for those clusters with no spectroscopic redshift). Figure 5 shows this comparison, and we find a photometric redshift error of $\delta z/(1+z) = 0.03$, consistent with B+18. As we detail above, we obtain photometric redshifts from $(g'-r')$ and $(r'-i')$ colours for clusters at low and high redshift, respectively; we show in Fig. 5 that clusters with $z_{\rm phot} < 0.45$ and $z_{\rm phot} > 0.45$ show the same rms dispersion, 0.033 in both cases. So, both $(g'-r')$ and $(r'-i')$ colours present a good behaviour to determine photometric redshifts.

4.2. Notes on individual clusters

In this section we provide a detailed description of the clusters listed in Table A.1 showing particular features, such as the presence of gravitational arcs and fossil systems, or even SZ counterparts reported by other authors or listed in other galaxy cluster catalogues. We note that all images shown in this section present north pointing upward and the east to the left.

Barrena et al. (2018) found several SZ sources associated with two or more clusters (multiple detections). For example, PSZ1 G075.29+26.66 includes two clusters, while PSZ1 G125.54−56.25 even encloses three clumps (see B+18). However, in the present work, we do not detect any SZ source showing multiple optical counterparts. Only PSZ1 G041.70+21.65 (ID-116) and PSZ1 G326.64+54.79 (ID-1140) may present some small galaxy groups very close to the *Planck* pointing. We identify small clumps at (RA = 17:47:26.63, Dec = +17:06:19.56) and (RA = 13 : 45 : 22.74, Dec = −05 : 34 : 41.01) in the ID-116 and ID-1140 fields, respectively. However, none of these galaxy clumps are rich enough to fit the richness selection criterion, and so not massive enough to be able to produce a SZ signal detectable by *Planck*. In agreement with Liu et al. (2015) (hereafter Liu+15), PSZ1 G041.70+21.65 shows a very massive optical counterpart at $z = 0.478$, which we observed spectroscopically using the OSIRIS/GTC MOS and we estimate a $\sigma_v > 1000\,{\rm km\,s^{-1}}$. PSZ1 G326.64+54.79 (ID-1140) also has a very rich counterpart, but still has to be observed spectroscopically to determine its velocity dispersion.

All the SZ counterparts positively validated and classified with `Flag`=1 have been spectroscopically confirmed as clusters with high velocity dispersion. In addition, we have decided to confirm the PSZ1 G205.52−44.21 (ID-677), validating it with `Flag`=1, although we have only one redshift for this cluster. The reason behind this decision is that the ID-677 counterpart is the Abell 471 cluster of galaxies, which was catalogued by Abell et al. (1989) as a (consolidated) very rich system.

PSZ1 G063.92−16.75 and PSZ1 G158.34−47.49. The SZ cluster counterparts are expected to be massive structures, and one observational proof supporting this is the existence of strong gravitational effects, such as arcs, in the core of the clusters. The clusters ID-209 and ID-554 are two examples of SZ counterparts showing gravitational arcs (see Fig. 6). Both clusters have been observed spectroscopically using OSIRIS/GTC MOS, finding 16 and 8 cluster members, respectively. The velocity dispersion estimate confirms that these two clusters are massive systems with $\sigma_v \sim 900\,{\rm km\,s^{-1}}$.

PSZ1 G097.52−14.92 and PSZ1 G249.14+28.98. The ID-340 and ID-846 clusters are two clear fossil systems, dominated by a huge central galaxy (see Fig. 7) and detected with high richness confidence ($\sigma_R \sim 5.8$). The systems are nearby clusters at $z_{\rm phot} = 0.04$ and 0.14, respectively. Neither of the clusters has been observed spectroscopically, so we have classified them as `Flag`=2.

Some of the SZ sources explored in this work, have also been studied by other authors, for example PSZ1 G051.42−26.16 (ID-162), which has been explored by vdB+16 using Megacam at CFHT. In agreement with vdB+16, we do not detect any cluster counterparts associated with this SZ source. In a similar way, Planck Collaboration Int. XXVI (2014) validate the PSZ1 G106.15+25.76 (ID-383) using the RTT150 telescope. Our estimation of $z_{\rm phot} = 0.60 \pm 0.04$ is in agreement with that obtained by Planck Collaboration Int. XXVI (2014) spectroscopically,

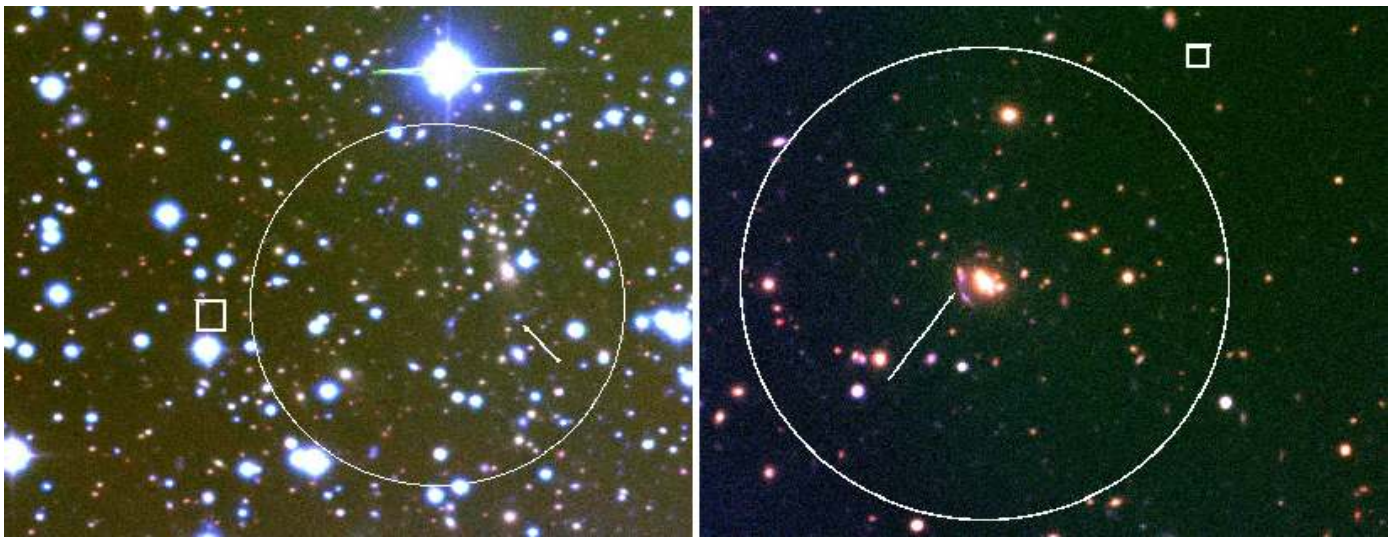

Fig. 6. RGB images obtained with the WFC/INT (*left*) and ACAM/WHT (*right*) g', r', and i' frames of the SZ sources PSZ1 G063.92−16.75 and PSZ1 G158.34−47.49, respectively. The squares indicate the corresponding SZ *Planck* coordinates, while the arrows point to the blue gravitational arcs detected in the core of the clusters. The circle is a 1.2′ radius region including the brightest galaxies of each cluster.

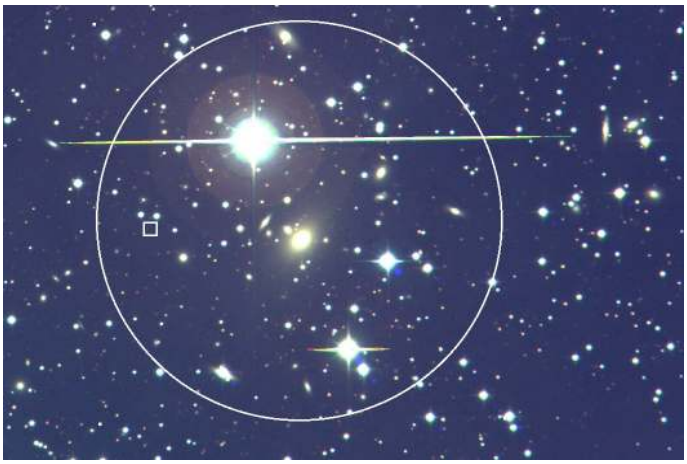

Fig. 7. Colour composite image obtained with the WFC/INT of the SZ source PSZ1 G097.52−14.92. The central dominant galaxy presents a magnitude $r' < 13$ and extends (up to surface brightness isophote $\mu_r = 25.5\,\mathrm{mag\,arcsec^{-2}}$) more than 2′ (∼100 kpc at the redshift of the cluster) from its centre. The circle encloses a 3′ radius region, where the majority of likely cluster members, showing $r' > 15$ mag are placed. The square marks the *Planck* SZ peak.

$z_{\rm spec} = 0.588$. In addition to this source, Planck Collaboration Int. XXVI (2014) confirms the ID-464 and ID-508. These two SZ sources are associated with high-redshift clusters at $z = 0.577$ and 0.820, respectively. In fact, PSZ1 G141.73+14.22 is one of the most distant cluster detected by *Planck*. We have observed ID-464 and 508 carrying out MOS with OSIRIS/GTC, and we estimate a $\sigma_v > 1100\,\mathrm{km\,s^{-1}}$ in both cases.

In agreement with Liu+15, we confirm spectroscopically the cluster at $z = 0.478$ as an actual counterpart of PSZ1 G041.70+21.65 (ID-116). We performed MOS with OSIRIS/GTC and, from 25 cluster members, we estimate a $\sigma_v > 1000\,\mathrm{km\,s^{-1}}$. For the source PSZ1 G306.96+50.58 (ID-1080), Liu+15 identify a galaxy overdensity at (RA = 13:01:46.1, Dec = −12 : 04 : 59), at 7.8′ to the north of the PSZ1 coordinates, which includes two bright galaxies, quite isolated, at $z_{\rm phot} = 0.21$. We find this galaxy clump showing a $\sigma_R < 0.5$, so very poor and compatible with the number of galaxies of the field. In addition, we also find a richer galaxy overdensity, showing a $\sigma_R \sim 3$, but at ∼6′ from the *Planck* pointing, compatible with a cluster at $z_{\rm phot} = 0.58$. However, following our selection criteria, this clump is too far from the *Planck* pointing (>5′) to be considered an actual counterpart. Thus, we classify this clump as `Flag`=3 and consequently, the ID-1080 PSZ1 source remains without a realistic cluster counterpart.

We also cross-correlate our target sample with other optically selected cluster catalogues, such as the catalogues by Wen et al. (2009, 2012). We find one match, which corresponds to WHL J35.5193+18.7745, associated with the PSZ1 G150.94−39.06 source. This is a very rich cluster ($\sigma_R = 9.9$) at $z_{\rm phot} = 0.21$ that we classify as `Flag`=2, awaiting spectroscopic validation in the near future.

4.3. Comments on non-detections

In our target sample there are several cases of clusters weakly associated with their corresponding SZ sources. These are the ID-111, 199, 372, 437, and 646. After prospecting them spectroscopically, we find small groups showing velocity dispersion in the range $\sigma_v = 300$−$500\,\mathrm{km\,s^{-1}}$, which are typical for low-mass clusters ($M_{500} \lesssim 10^{14}\,M_\odot\,h_{70}^{-1}$), so they do not fit our selection criteria. In particular, the ID-646 source seems to be a very clumpy system (very substructured) at $z = 0.24$, and not very rich ($\sigma_R = 3$), which shows signs of being a low-mass system, with a $\sigma_V \sim 300\,\mathrm{km\,s^{-1}}$ (obtained with a few spectra available in the SDSS-DR12 archive).

In addition, we study in detail two cases, ID-85 and ID-743, where no clusters or even poor groups have been identified, and hence in order to validate them as actual counterparts they have to be explored spectroscopically. In the first case, in addition to the WFC/INT image, we observed this field using GTC/OSIRIS imaging mode, and obtained an image 1.5 mag deeper than the WFC/INT image. The GTC image reveals that no galaxy overdensity can be associated with this SZ source. For the case of ID-743, we perform OSIRIS/GTC MOS observations and we do not identify any actual galaxy concentration associated with this SZ source. However, Liu+15 validate this source as a clump

of galaxies at $z = 0.381$ that we also detect in the INT/WFC images as a poor group of galaxies with $\sigma_R < 1.5$. Consequently, we classify this SZ source as 'ND' showing no actual cluster counterparts.

Following the validation criteria described in Sect. 3, we find 49 sources showing no galaxy overdensity. This means that ∼65% of the SZ sources analysed in this work show no optical counterpart. In general, the ITP13 has found optical counterparts for 55% (140/256) of the SZ sources studied, while 45% (116/256) remain with unconfirmed counterparts. There are three possible explanations for so many non-detections. First, there could be counterparts at very high redshift ($z > 0.85$) that can only be detected using near-infrared images; second, the *Planck* SZ detection could be affected by the Eddington bias (Eddington 1913; vdB+16). The third possibility is related to the contamination produced by the non-Gaussianity noise of foreground sources.

The detection of clusters at $z > 0.85$ using the *Planck* SZ maps is not very efficient at such high redshift. Only a few high-redshift clusters have been detected (see e.g. Burenin et al. 2018; vdB+16). The ITP13 observations are performed using broad-band filters in the visible wavelength range, up to 8200 Å, so the detection of galaxy clusters is restricted up to $z < 0.85$ in this programme. However, the detection of a few high-redshift clusters does not explain the presence of so many SZ sources with unconfirmed counterparts (116 PSZ1 sources; see Sect. 5).

The second possibility is that the large fraction of non-detections is related to the Eddington bias, which is a statistical effect that arises when a threshold in S/N is imposed in a detection procedure. This may introduce false SZ dectection in the low SZ S/N regime (∼4.5−5.5), and low-mass haloes may be detected.

A substantial number of SZ sources, mostly detected with very low SZ significance, present very irregular and elongated contour shapes of SZ emission. Figure 8 illustrates, an example of one such case. These cases can be typical candidates affected by Eddington bias. As Streblyanska et al. (2018) show (see Fig. 2 therein), the Compton y-maps[8] of a large fraction of SZ sources classified as non-detection present very irregular shapes and no obvious peak at the nominal position of the *Planck* sources.

However, the Eddington bias by itself cannot explain the large fraction of SZ sources with unconfirmed counterparts because the dectection of poor systems (with $M_{500} < 10^{14}\, M_\odot\, h_{70}^{-1}$) at low redshift ($z < 0.3$) is insignificant or even null.

For the third option the influence of thermal radio emission of cold galactic dust is explored in detail in Sect. 5. We statistically study the correlation between high diffuse radio emission zones with unconfirmed SZ sources, providing new and detailed information on the completeness and purity of the PSZ1 sample.

5. PSZ1 statistics: purity and contamination

In this section we analyse the statistical properties of the northern PSZ1 sample in order to obtain conclusions related to the full PSZ1 catalogue. With the purpose of comparing the PSZ1 sample with the one observed in the ITP13 programme, we selected PSZ1 sources with Dec $\geq -15°$, and we named it PSZ1-North. The PSZ1-North sample contains 753 SZ sources (61% of the full PSZ1 catalogue) which is divided in two different subsets. The first includes 541 sources already validated at the time of the first PSZ1 publication in 2013 (Planck Collaboration XXXII 2015) and other optical follow-up programmes, such as that performed with the RTT150 telescope (Planck Collaboration Int. XXVI 2014). We refer to this as the PSZ1-Val sample. The second, called the ITP13 sample, is composed of the 212 sources that we observed during the ITP13 optical follow-up programme.

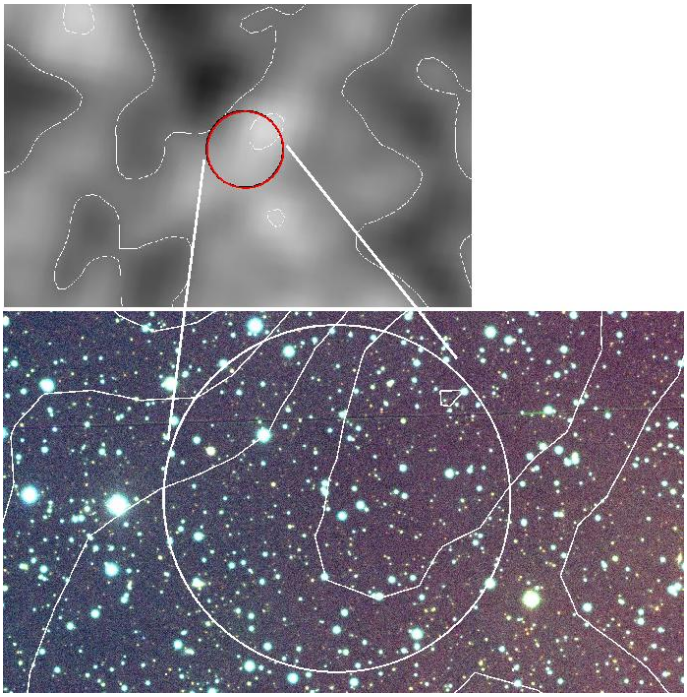

Fig. 8. *Upper panel*: MILCA Compton y-maps in the area around the SZ source PSZ1 G012.66+25.79 (ID-34 showing a 4.5 SZ significance). *Lower panel*: RGB image in the region around PSZ1 G012.66+25.79. The circle encloses the 5′ region centred on the PSZ1 coordinates of this SZ source. The white contours correspond to the SZ emission at 2σ, 3σ, and 4.5σ detection levels.

Figure 9 shows the number of clusters normalised to the total PSZ1-North clusters, and Table 3 reports the summary information of the full IT13 programme. The first column specifies the corresponding ITP13 year and reference. Columns 2, 3, and 4 list the number of PSZ1 sources observed, confirmed, and spectroscopically studied, respectively. The remaining columns provide the cluster counts according to the confirmation criteria adopted here.

The ITP13 programme studied a total of 256 sources, 212 of which were completely unknown and 44 had no spectroscopic redshift. In the end, we positively confirmed 140 optical counterparts and 116 remain unconfirmed. In addition, 126 PSZ1 sources at low SZ S/N were studied spectroscopically in the redshift range $0.02 < z < 0.85$. The ITP13 confirmed 11 cluster counterparts at $z > 0.7$, which implies 80% of the PSZ1-North sources at this redshift, and all four clusters at $z > 0.8$. Moreover, we were able to study 30 clusters showing redshifts $z > 0.5$, which means 55% of the PSZ1-North sample at high redshift.

The left panel of Fig. 10 shows the distribution of PSZ1-North sources as function of SZ S/N detection. From the histogram we obtain a median value for $\langle S/N \rangle = 5.1$, which is comparable to the value that we found for the ITP13 sample ($S/N = 4.9$).

[8] Full-sky Compton parameter (y-map) was obtained using the MILCA procedure (Planck Collaboration XXI 2014) which has been publicly available since 2015 (Planck Collaboration XXII 2016).

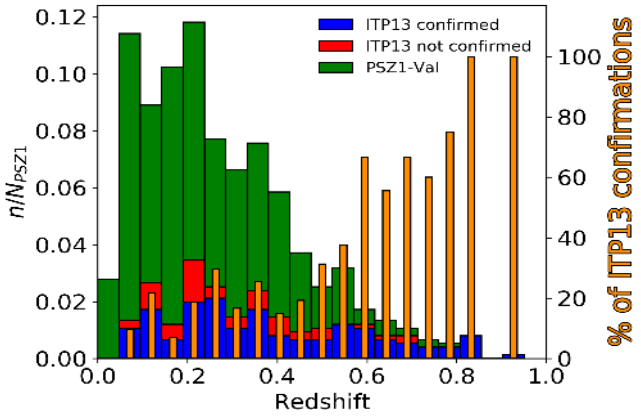

Fig. 9. Fraction of PSZ1 sources as a function of redshift and normalised to the total number of PSZ1-North sources. The PSZ1-Val sample is represented in green. Blue and red bars correspond to the ITP sample, classified as confirmed (with `Flag`=1 and 2) and unconfirmed (`Flag`=3) sources, respectively. Orange vertical bars show the fraction of SZ sources confirmed during the full ITP13 programme.

We can summarise all this information with accumulated purity. Here we define the purity as the fraction of confirmed clusters with respect to the total number of SZ sources. In Fig. 10, right panel, we show how this purity behaves as a function of S/N. From this analysis, we conclude that, after all validation programmes, the purity of the PSZ1-North sample has passed from 72% to 83%, especially at very low S/N, due to the efforts performed in the ITP13 optical follow-up, providing new cluster confirmations. It is important to note that the purity of the original PSZ1-North sample (red line) and of the full PSZ1 catalogue (orange line) are compatible. This allows us to extrapolate our results (in terms of fraction of ND and statistical completeness and purity) to the full PSZ1 catalogue. So, in this sense, the actual purity of PSZ1 catalogue here obtained (blue curve in Fig. 10) can be qualitatively compared with the simulated catalogue estimated for the original PSZ1 sample (see Fig. 10. in Planck Collaboration XXIX 2014). The two curves follow a very similar shape and, after completing the ITP13 optical follow-up, we can affirm that the PSZ1 presents a ∼83% statistical reliability at $S/N = 4.5$ detection, which is fully compatible with the value of 84% estimated in Planck Collaboration XXIX (2014). In addition, we see how the final PSZ1 reliability is even better than predicted for sources with S/N between 7 and 12, being 100% pure for detections with $S/N > 9$. We have to take into account these findings in a qualitative way, mainly because many PSZ1 unconfirmed sources in the southern sky still remain without any validation.

We note that the percentage of unconfirmed sources in the low S/N half (<5.1) of the ITP-North sample is 23.4%, whereas for $S/N \geq 5.1$ this same fraction is only 9.5%. Here, we explore whether these findings could be explained in terms of dust contamination in the *Planck* SZ detections. We studied these sources in detail looking at the radio emission in the 857 GHz *Planck* map. In fact, B+18 found hints suggesting that thermal dust emission may hardly influence the SZ signal (see Sect. 4.3 therein). This effect may produce false SZ detections, especially around regions showing dense galactic dust clouds or even high extinction.

Figure 11 shows how the fraction of non-validated sources (`Flag`= 3 and ND) with respect to the total number of PSZ1-North sample sources (red squares), correlates with the signal at 857 GHz[9], computed as the mean signal within a region of 0.5° around the nominal PSZ1 coordinates. In the regions where the dust contamination is very low (<5 MJy sr^{-1}), the fraction of unconfirmed sources is well below 20%. However, fields with high dust emission also show high fractions (>60%) of non-detections. Moreover, taking into account the $S/N \leq 5.1$ (dark blue line) and the $S/N > 5.1$ (light blue line) bins separately, we note that ∼100% of low SZ S/N sources that show a very high contamination (>13 MJy sr^{-1}) are non-validated.

This effect, produced by the cold galactic dust and thus correlated to the galactic latitude (see Fig. 11, right panel), has an important effect on the selection function of the SZ detections using the *Planck* maps. In particular, we find that the fraction of unconfirmed sources at low galactic latitudes ($|b| < 20°$) can be as high as 27%, while at high galactic latitudes ($|b| > 60°$) is lower than 10%. We exclude from this analysis the SZ sources placed at $|b| > 75°$ because of the low number of targets at this high galactic latitude. While the number of SZ sources per bin is between 80 and 160 at $|b| < 75°$, this number count drops up to 17 sources at $|b| > 75°$, making this study not statistically significant (i.e. with errors larger than 100%) in this range.

Summarising, our findings confirm that the fraction of PSZ1 false detections is dominated by non-Gaussian noise in the foreground signal, in particular Galactic dust emission, as originaly predicted by Planck Collaboration XXIX (2014) (see Fig. 11 therein).

6. Conclusions

This article is the third work in the framework of the ITP13 PSZ1 validation programme and represents the last in a series of three papers (see also Planck Collaboration Int. XXXVI 2016 and B+18) aiming to carry out the optical validation of unknown SZ counterparts. The work presented here shows the results obtained in the second year of the ITP13 (August 2013 to July 2015) dedicated to characterising unknown PSZ1 sources in the northern sky (with Dec $\geq -15°$) from optical/visible facilities installed at the ORM.

We analysed 75 PSZ1 sources by obtaining deep imaging and spectroscopic data, mostly MOS, which allow us to study the nature of the detected systems through their 2D galaxy distribution, redshifts, and velocity dispersion. We assumed a robust confirmation criteria (based on the distance to the PSZ1 coordinates, richness, and velocity dispersion) in order to validate cluster counterparts, and labelled them following a scheme of flags. So, clusters labelled `Flag`=1 and 2 are confirmed clusters. The first set corresponds to definitive cluster counterparts and the second set to those waiting for velocity dispersion and redshift estimates. False detections are considered clusters, with `Flag`=3 and ND. The former are galaxy overdensities very far from the PSZ1 centre or poor systems which do not allow a realistic association with the SZ signal. The latter are simply SZ sources with no cluster counterparts.

Following this classification, we find 26 confirmed counterparts and 49 unconfirmed detections. So, one-third of the sample analysed in this work show actual cluster counterparts. This small fraction of SZ sources with cluster counterparts is mainly due to the low SZ S/N of the target considered. We find a clear relation between the fraction of SZ sources catalogued as non-detections with the thermal emission at 857 GHz produced by the cold galactic dust. In particular, we find that almost all

[9] We use here the full-mission 857GHz *Planck* maps as downloaded from `http://pla.esac.esa.int/pla/`

Table 3. Summary information of the full ITP13 programme.

Programme/Reference	Observed	Confirmed(*)	Spec	Flag=1	Flag=2	Flag=3	ND
PC36 (**)	66	61	42	(***)	(***)	(***)	5
ITP13 year 1/B+18	115	53	56	25	28	13	49
ITP13 year 2/this work	75	26	28	16	10	12	37
Total	256	140	126	>41	>38	>25	91

Notes. (*)Total confirmed clusters correspond to the sum of counts with Flag=1 and Flag=2. (**)PC36 corresponds to Planck Collaboration Int. XXXVI (2016), which was developed as a previous observational programme. (***)No flag classification was performed by PC36, and SZ sources were classified as "confirmed" and "non-detections". So, total counts in Cols. 5, 6, and 7 represent minimum values.

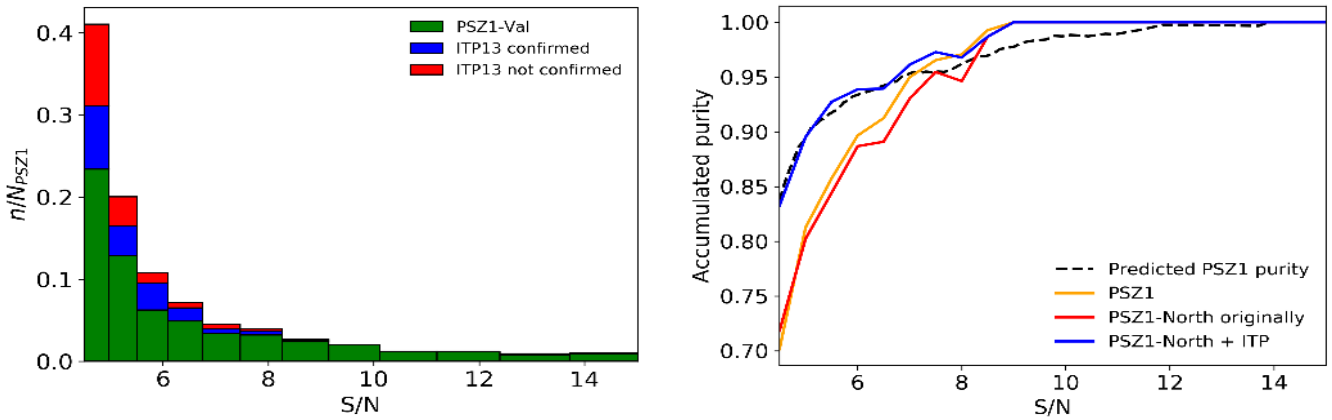

Fig. 10. *Left panel*: cluster counts of PSZ1-North sources as a function of the SZ S/N detection. The PSZ1-Val sample is represented in green, which includes SZ validated sources in all previous follow-up programmes. The confirmed clusters within the ITP13 sample are shown in blue, whereas non-validated clusters (classified as Flag=3 and ND) are shown in red. *Right panel*: fraction of confirmed clusters as a function of the S/N in the PSZ1-North sample. The red line represents the purity at the moment of the publication of the PSZ1 catalogue and blue line shows the purity after completing the ITP13 follow-up. The orange line represents the accumulated purity of the full PSZ1 catalogue at the moment of its first publication, while the black dashed line is the predicted PSZ1 reliability retrived from Planck Collaboration XXIX (2014) (see Fig. 10 therein).

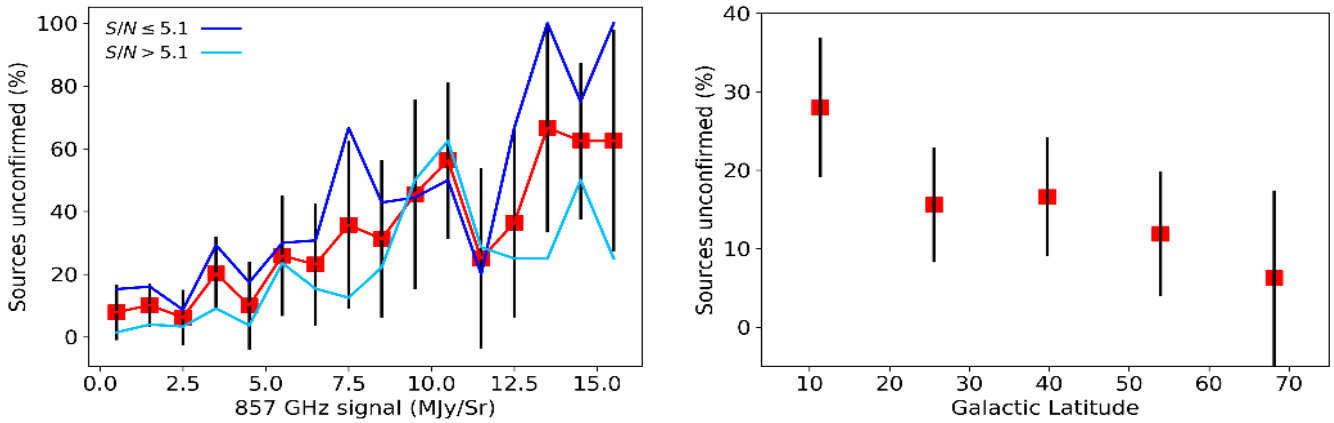

Fig. 11. *Left panel*: fraction of unconfirmed sources with respect to the total number of elements of the PSZ1-North sample (Dec $\geq -15°$) as a function of the 857 GHz signal in MJy sr^{-1} taking into account the entire sample (red squares), the $S/N < 5.1$ subsample (dark blue line), and the $S/N \geq 5.1$ subsample (light blue line). *Right panel*: percentage of unconfirmed sources with respect the total number of elements of the PSZ1-North sample as a function of the galactic latitude. The error bars represents the Poisson uncertainty of the total number of sources in each bin.

the low SZ S/N sources (≤5.1) showing >13 MJy sr^{-1} are non-detections. Thus, this contamination effect statistically correlates with the galactic latitude, which confirms that the selection funcion of SZ detections on *Planck* maps displays significant variations over different sky areas.

We were able to characterise 212 (validating positively 140 of them) SZ sources, which means 28% of the PSZ1 sources previously unknown at Dec $\geq -15°$. In total, we provided 172 and 126 photometric and spectroscopic redshifts of PSZ1 sources, respectively. The contribution of the ITP13 programme was especially important for confirming high-redshift cluster counterparts. In this sense, 55% (80%) of the clusters with $z > 0.5$ ($z > 0.7$) have been confirmed in the ITP13 framework. The ITP13 results have contributed to characterising 17% of the full PSZ1 sample.

The results derived from the ITP13 programme have allowed us to obtain a more precise knowledge of the PSZ1 purity, confirming that this sample is ~83% pure for detections at 4.5 SZ significance. So, the ITP13 has provided a better understanding of the SZ *Planck* detections, demonstrating that, as originally predicted, false detections are clearly dominated by non-Gaussianity noise of foreground signal.

A similar work has been continued with an additional two-year observational programme, the LP15, dedicated to validating PSZ2 sources in the northern hemisphere from the Canary Islands observatories (see Streblyanska et al. 2019; Aguado-Barahona et al. 2019).

New observational programmes are planned in order to ultimately confirm additional clusters. In addition, in a future work, we will provide the dynamical masses obtained from velocity dispersions for the clusters reported here in order to obtain an accurate estimation of the mass bias parameter, $(1 - b)$, as an attempt to shed some light on the mass scale relation ($M_{\rm SZ}/M_{\rm true}$). This would allow us to improve the determination of cosmological parameters (mainly σ_8 and $\Omega_{\rm m}$) using the cluster abundance.

Acknowledgements. This article is based on observations made with (a) the Gran Telescopio Canarias operated by the Instituto de Astrofísica de Canarias, (b) the *Isaac Newton* Telescope, and the *William Herschel* Telescope operated by the Isaac Newton Group of Telescopes, and (c) the Italian Telescopio Nazionale *Galileo* operated by the Fundación Galileo Galilei of the INAF (Istituto Nazionale di Astrofisica). All these facilities are located at the Spanish del Roque de los Muchachos Observatory of the Instituto de Astrofísica de Canarias on the island of La Palma. This research has been carried out with telescope time awarded by the CCI International Time Programme at the Canary Islands Observatories (programmes ITP13B-15A). Funding for the Sloan Digital Sky Survey (SDSS) has been provided by the Alfred P. Sloan Foundation, the Participating Institutions, the National Aeronautics and Space Administration, the National Science Foundation, the U.S. Department of Energy, the Japanese Monbukagakusho, and the Max Planck Society. HL is funded by PUT1627 grant from the Estonian Research Council and by the European Structural Fundsgrant for the Centre of Excellence "Dark Matter in (Astro)particle Physics and Cosmology" TK133. AAB, AF, AS, RB, DT, RGS, and JARM acknowledge financial support from Spain's Ministry of Economy and Competitiveness (MINECO) under the AYA2014-60438-P and AYA2017-84185-P projects. MR acknowledges financial support from contract ASI-INAF n. 2017-14-H.0.

References

Abell, G. O. 1958, ApJS, 3, 212
Abell, G. O., Corwin, H. G., Jr, & Olowin, R. P. 1989, ApJS, 70, 1
Aguado-Barahona, A., Barrena, R., Streblyanska, A., et al. 2019, A&A, 631, A148
Aihara, H., Allende-Prieto, C., An Deokkeun, D., et al. 2011, ApJS, 193, 29
Allen, S. W., Evrard, A. E., & Mantz, A. B. 2011, ARA&A, 49, 409
Barrena, R., Streblyanska, A., Ferragamo, A., et al. 2018, A&A, 616, A42
Bertin, E., & Arnouts, S. 1996, A&AS, 117, 393
Bleem, L. E., Stalder, B., & De Haan, T. 2015, ApJS, 216, 27
Boada, S., Hughes, J. P., Menanteau, F., et al. 2019, ApJ, 871, 188
Böhringer, H., Voges, W., Huchra, J. P., et al. 2000, ApJS, 129, 435
Böhringer, H., Chon, G., Collins, C. A., et al. 2013, A&A, 555, A30
Borgani, S., & Guzzo, L. 2001, Nature, 409, 39
Burenin, R. A., Bikmaev, I. F., Khamitov, I. M., et al. 2018, Astron. Lett., 44, 297
Carlstrom, J. E., Holder, G. P., & Reese, E. D. 2002, ARA&A, 40, 643
Carlstrom, J. E., Ade, P. A. R., Aird, K. A., et al. 2011, PASP, 123, 568
Cutri, R. M., Wright, E. L., Conrow, T., & at., 2012, Explanatory Supplement to the WISE All-Sky (Data Release Products)
Donahue, M., Voit, G. M., Gioia, I., et al. 1998, ApJ, 502, 550
Ebeling, H., Edge, A. C., Bohringer, H., et al. 1998, MNRAS, 301, 881
Eddington, A. S. 1913, MNRAS, 73, 359
Eke, V. R., Cole, S., & Frenk, C. 1996, MNRAS, 282, 263
Evrard, A. E. 1989, ApJ, 341, L71
Fort, B., Mellier, Y., Picat, J.-P., & at., 1986, Proc. SPIE, 627, 321
Gladders, M. D., & Yee, H. K. C. 2000, AJ, 120, 2148
Gonzalez, A. H., Gettings, D. P., et al. 2019, ApJS, 240, 33
Henry, J. P., & Arnaud, K. A. 1991, ApJ, 372, 410
Jones, L. R., Ponman, T. J., et al. 2003, MNRAS, 343, 627
Liu, J., Hennig, C., Desai, S., et al. 2015, MNRAS, 449, 3370
Mantz, A., Allen, S. W., Rapetti, D., & Ebeling, H. 2010, MNRAS, 406, 1759
Mamon, G., Biviano, A., & Murante, G. 2010, A&A, 520, A30
Marriage, T. A., Acquaviva, V., Ade, P. A. R., et al. 2011, ApJ, 737, 61
Melin, J. B., Aghanim, N., Bartelmann, M., et al. 2012, A&A, 548, A51
Munari, E., Biviano, A., Borgani, S., et al. 2011, MNRAS, 430, 2638
Piffaretti, R., Arnaud, M., Pratt, G. W., et al. 2011, A&A, 534, A109
Planck Collaboration VIII. 2011, A&A, 536, A8
Planck Collaboration I. 2014, A&A, 571, A1
Planck Collaboration XXI. 2014, A&A, 571, A21
Planck Collaboration XXIX. 2014, A&A, 571, A29
Planck Collaboration XXXII. 2015, A&A, 581, A14
Planck Collaboration XXIV. 2016, A&A, 594, A24
Planck Collaboration XXVII. 2016, A&A, 594, A27
Planck Collaboration XXII. 2016, A&A, 594, A22
Planck Collaboration Int. XXVI. 2014, A&A, 582, A29
Planck Collaboration Int. XXXVI. 2016, A&A, 586, A139
Postman, M., Lubin, L. M., & Gunn, J. E. 1996, AJ, 111, 615
Soucail, G., Fort, B., Mellier, Y., et al. 1987, A&A, 172, L14
Streblyanska, A., Barrena, R., Rubiño-Martín, J. A., et al. 2018, A&A, 617, A71
Streblyanska, A., Aguado-Barahona, A., Ferragamo, A., et al. 2019, A&A, 628, A13
Sunyaev, R. A., & Zeldovich, Y. B. 1972, Comm. Astrophys. Space Phys., 4, 173
Swetz, D. S., Ade, P. A. R., Amiri, M., et al. 2011, ApJS, 194, A41
Tonry, J., & Davis, M. 1979, AJ, 84, 1511
van der Burg, R. F. J., Aussel, H., Pratt, G. W., et al. 2016, A&A, 587, A23
Vikhlinin, A., Kravtsov, A. V., Burenin, R. A., et al. 2009, ApJ, 692, 1060
Voevodkin, A., Borozdin, K., et al. 2010, ApJ, 708, 1376
Voges, W., Aschenbach, B., Boller, T., et al. 1999, A&A, 349, 389
Voges, W., Aschenbach, B., Boller, T., et al. 2000, IAU Circ., 7432, 3
Wen, Z. L., Han, J. L., & Liu, F. S. 2009, ApJS, 183, 197
Wen, Z. L., Han, J. L., & Liu, F. S. 2012, ApJS, 199, 34
White, S. D. M., Navarro, J. F., Evrard, A. E., et al. 1993, Nature, 6454, 433
Wittman, D., Dell'Antonio, I. P., Hughes, J. P., et al. 2006, ApJ, 643, 128
Wright, E. L., Eisenhardt, P. R. M., Mainzer, A. K., et al. 2010, AJ, 140, 1868
Zohren, H., Schrabback, T., van der Burg, R. F. J., et al. 2019, MNRAS, 488, 2523

Table A.1. Clusters counterparts and PSZ1 sources studied in this work.

ID		*Planck* name	SZ S/N	RA	Dec	Dist. (′)	$\langle z_{\rm spec}\rangle$; $z_{\rm spec,BCG}$	$N_{\rm spec}$	$z_{\rm phot}$	R_c ; σ_R	Flag	Notes
PSZ1	PSZ2			(J2000)								
32		PSZ1 G012.48+27.36	4.54	–	–	–	–	–	–	–	ND	
34		PSZ1 G012.66+25.79	4.50	–	–	–	–	–	–	–	ND	
38		PSZ1 G015.42+58.42	4.65	–	–	–	–	–	–	–	ND	
85	111	PSZ1 G031.44−19.16	4.60	–	–	–	–	–	–	–	ND	
111		PSZ1 G040.17−41.51	4.57	21 32 51.93	−12 32 33.42	5.95	0.229 ; 0.2264	9	0.22 ± 0.03	7.0 ; 1.8	3	
112		PSZ1 G040.33−16.55	4.61	–	–	–	–	–	–	–	ND	
116	151	PSZ1 G041.70+21.65	4.51	17 47 09.18	+17 11 01.67	4.77	0.478 ; 0.4773	25	0.45 ± 0.05	9.0 ; 2.8	1	Liu+15
132		PSZ1 G045.44−08.73	4.57	–	–	–	–	–	–	–	ND	
135	175	PSZ1 G045.85+57.71	5.32	15 18 20.55	+29 27 40.50	0.39	0.607 ; 0.6094	37	0.66 ± 0.03	39.0 ; 6.2	1	
149	192	PSZ1 G048.22−51.60	4.50	22 20 17.44	−12 11 30.03	1.93	0.530 ; 0.5322	30	0.52 ± 0.02	7.5 ; 2.7	1	
162		PSZ1 G051.42−26.16	4.60	–	–	–	–	–	–	–	ND	vdB+16
193		PSZ1 G058.77−26.14	4.55	–	–	–	–	–	–	–	ND	
199		PSZ1 G059.99+11.06	4.55	19 00 19.37	+28 58 09.73	4.21	0.097 ; 0.0974	12	0.04 ± 0.03	12.0 ; 4.3	3	
203		PSZ1 G060.51−19.54	4.65	20 54 31.65	+13 38 05.57	2.04	–	–	0.59 ± 0.05	9.0 ; 3.0	2	
209	264	PSZ1 G063.92−16.75	4.62	20 52 51.70	+17 54 23.02	1.73	0.392 ; 0.3923	16	0.36 ± 0.04	46.2 ; 5.8	1	Gravitational arc
211		PSZ1 G064.30+30.58	4.58	–	–	–	–	–	–	–	ND	
212		PSZ1 G064.83+35.79	4.54	17 10 08.52	+40 20 53.64	4.35	0.442 ; 0.4429	22	0.46 ± 0.04	14.8 ; 6.5	1	
276		PSZ1 G083.35+76.41	4.65	–	–	–	–	–	–	–	ND	
311		PSZ1 G091.73−30.23	4.53	–	–	–	–	–	–	–	ND	
332	438	PSZ1 G095.00−37.14	4.53	–	–	–	–	–	–	–	ND	
340	456	PSZ1 G097.52−14.92	5.06	22 37 21.21	+41 15 01.48	2.59	–	–	0.04 ± 0.02	32.0 ; 5.7	2	Fossil system
346	462	PSZ1 G098.42+77.25	4.71	13 18 42.87	+38 43 00.13	9.90	0.234 ; 0.2348	18	0.23 ± 0.02	27.1 ; 3.3	3	
371		PSZ1 G103.24+16.92	4.55	–	–	–	–		–	–	ND	
372		PSZ1 G103.50+31.36	4.63	17 36 44.28	+72 34 34.07	1.35	0.226 ; 0.2257	18	0.24 ± 0.04	7.4 ; 2.7	3	
373*		PSZ1 G103.56−39.35	4.50	23 47 12.69	+21 06 02.64	5.68	0.488 ; 0.4877	1	0.44 ± 0.03	3.9 ; 1.5	3	
383	513	PSZ1 G106.15+25.76	4.64	18 56 51.95	+74 55 52.73	0.58	–	–	0.60 ± 0.04	10.0 ; 3.2	2	PC26+
398		PSZ1 G109.09−52.45	4.55	–	–	–	–	–	–	–	ND	
430		PSZ1 G117.29+13.44	4.54	23 22 12.90	+75 19 28.74	2.15	0.466 ; 0.4677	31	0.49 ± 0.04	16.0 ; 3.6	1	
437	579	PSZ1 G118.87+42.71	4.51	13 35 21.87	+74 04 10.10	1.30	0.215 ; –	8	0.17 ± 0.03	12.0 ; 1.4	3	
450	604	PSZ1 G123.39+30.62	4.53	12 24 40.09	+86 27 46.51	1.25	0.200 ; 0.1979	9	0.29 ± 0.03	19.6 ; 4.4	1	
455		PSZ1 G124.56+25.38	4.76	–	–	–	–	–	–	–	ND	
464	630	PSZ1 G127.02+26.21	4.95	05 58 02.70	+86 13 49.31	1.33	0.577 ; 0.5760	13	0.63 ± 0.05	20.0 ; 5.0	1	
483*		PSZ1 G134.75−56.53	4.57	01 17 21.05	+05 46 08.09	3.39	0.206 ; 0.2077	11	0.21 ± 0.03	20.0 ; 5.0	1	
489		PSZ1 G135.68+45.61	4.58	–	–	–	–	–	–	–	ND	

Notes. (*)Studied using SDSS-DR12 photometric and/or spectroscopic data. (+)PC26 acronism corresponds to Planck Collaboration Int. XXVI (2014).

Table A.1. continued.

ID		*Planck* name	SZ S/N	RA	Dec	Dist. ($'$)	$\langle z_{\rm spec}\rangle$; $z_{\rm spec,BCG}$	$N_{\rm spec}$	$z_{\rm phot}$	R_c ; σ_R	Flag	Notes
PSZ1	PSZ2			(J2000)								
507	688	PSZ1 G141.59+23.69	4.83	06 23 55.16	+72 50 15.69	8.97	0.306 ; 0.3071	14	0.26 ± 0.03	10.9 ; 4.8	3	
508	689	PSZ1 G141.73+14.22	4.97	04 41 05.88	+68 13 15.13	0.96	0.820 ; 0.8208	19	0.78 ± 0.06	– ; –	1	PC26^{+}
515	699	PSZ1 G143.70−08.59	4.56	–	–	–	–	–	–	–	ND	
517		PSZ1 G144.99+54.39	4.63	11 14 21.86	+58 23 19.76	11.36	0.206 ; 0.2063	25	0.21 ± 0.02	30.0 ; 5.5	3	
536$^{(*)}$	733	PSZ1 G150.94−39.06	5.09	02 22 04.63	+18 46 28.10	3.22	–	–	0.21 ± 0.02	29.2 ; 9.9	2	WHL J35.5193+18.7745
538		PSZ1 G151.44−64.86	4.70	01 38 13.13	−04 30 50.78	7.20	0.158 ; 0.1583	2	0.15 ± 0.03	11.0 ; 1.8	3	Long-slit spectroscopy
554	762	PSZ1 G158.34−47.49	4.63	02 24 56.13	+08 49 47.59	2.17	0.311 ; 0.3115	8	0.29 ± 0.01	7.6 ; 2.8	1	Gravitational arc
555		PSZ1 G158.58−52.47	4.51	–	–	–	–	–	–	–	ND	
557		PSZ1 G159.29−24.66	4.76	03 21 00.12	+27 26 50.70	0.29	–	–	0.56 ± 0.05	12.0 ; 3.5	2	
559		PSZ1 G160.59+17.41	4.67	06 21 11.30	+53 56 33.81	2.87	–	–	0.33 ± 0.04	24.0 ; 4.9	2	
566	775	PSZ1 G163.03−27.80	4.50	–	–	–	–	–	–	–	ND	
590		PSZ1 G171.01+15.93	4.89	06 35 47.93	+44 10 15.14	1.36	0.281 ; 0.2823	20	0.28 ± 0.03	12.1 ; 3.5	1	
597	819	PSZ1 G173.07−36.12	4.95	–	–	–	–	–	–	–	ND	
611		PSZ1 G181.12−29.42	4.82	–	–	–	–	–	–	–	ND	
625	858	PSZ1 G185.53−33.97	4.98	–	–	–	–	–	–	–	ND	
629		PSZ1 G186.54+85.60	4.51	–	–	–	–	–	–	–	ND	
639		PSZ1 G189.29+07.44	5.10	06 34 44.47	+24 20 42.31	2.65	0.504 ; 0.5041	4	0.55 ± 0.05	7.3 ; 1.8	2	Long-slit spectroscopy
645		PSZ1 G191.05+12.85	4.51	06 59 50.96	+25 05 20.20	4.10	0.088 ; 0.0895	15	0.07 ± 0.04	36.3 ; 7.1	1	
646	880	PSZ1 G191.78−26.64	4.76	04 38 54.25	+04 49 18.16	8.20	0.206 ; 0.2082	4	0.24 ± 0.04	9.0 ; 3.0	3	Long-slit spectroscopy
652		PSZ1 G194.70−58.93	4.62	–	–	–	–	–	–	–	ND	
656	897	PSZ1 G196.62−45.50	4.72	03 42 54.55	−08 41 08.18	3.04	–	–	0.25 ± 0.03	88.0 ; 9.4	2	
659		PSZ1 G198.06−12.52	4.82	–	–	–	–	–	–	–	ND	
663	906	PSZ1 G199.70+37.01	4.89	–	–	–	–	–	–	–	ND	
671		PSZ1 G203.42−04.03	4.70	–	–	–	–	–	–	–	ND	
677		PSZ1 G205.52−44.21	4.60	03 59 32.89	−13 39 56.41	2.33	0.252 ; 0.2523	1	0.31 ± 0.03	27.0 ; 5.2	1	Abell 471 (L-S spectroscopy)
698		PSZ1 G212.63+07.45	4.72	–	–	–	–	–	–	–	ND	
699		PSZ1 G212.80+46.65	4.77	–	–	–	–	–	–	–	ND	
743		PSZ1 G223.80+58.50	4.57	–	–	–	–	–	–	–	ND	Liu+15
748		PSZ1 G224.45+05.25	4.55	07 31 13.82	−07 48 33.48	4.47	0.067 ; 0.0670	17	0.06 ± 0.03	41.0 ; 6.4	1	
753		PSZ1 G225.39+04.23	4.52	–	–	–	–	–	–	–	ND	
786	1065	PSZ1 G234.12+10.45	4.61	08 09 04.96	−13 30 29.30	2.03	0.294 ; 0.2979	27	0.45 ± 0.04	52.0 ; 7.2	1	
791$^{(*)}$	1070	PSZ1 G235.93+38.21	4.79	09 46 34.48	+00 28 02.13	6.66	0.455 ; 0.4507	2	0.47 ± 0.03	5.0 ; 0.8	3	
798		PSZ1 G237.94+21.65	5.05	–	–	–	–	–	–	–	ND	
809		PSZ1 G240.42+77.58	4.59	–	–	–	–	–	–	–	ND	
846		PSZ1 G249.14+28.98	4.74	09 44 57.58	−13 48 11.22	1.36	–	–	0.14 ± 0.03	34.0 ; 5.8	2	Fossil System
900		PSZ1 G262.45+49.34	4.60	–	–	–	–	–	–	–	ND	
928		PSZ1 G268.86+55.92	4.66	–	–	–	–	–	–	–	ND	
1080		PSZ1 G306.96+50.58	4.61	13 01 37.25	−12 08 21.58	5.94	–	–	0.58 ± 0.04	6.6 ; 2.9	3	Liu+15
1140	1539	PSZ1 G326.64+54.79	6.61	13 45 14.72	−05 32 04.03	3.02	–	–	0.46 ± 0.05	44.0 ; 6.6	2	
1199		PSZ1 G346.57+42.71	4.60	–	–	–	–	–	–	–	ND	
1217		PSZ1 G355.14+55.96	4.52	–	–	–	–	–	–	–	ND	